Research Square

Preprints are preliminary reports that have not undergone peer review.
They should not be considered conclusive, used to inform clinical practice,
or referenced by the media as validated information.

Multi-model study on the influence of arc additive manufacturing process parameters on the morphology of the molten pool

Yuhao Zeng
Dongguan University of Technology
Tinghua Ou
1828941857@qq.com

Dongguan University of Technology https://orcid.org/0009-0003-9915-3479
Xin Shang
Dongguan University of Technology
Lijuan Pang
Panzhihua University
Yansong Huang
Dongguan University of Technology
Zeyu Yang
Dongguan University of Technology
Dongyu Liu
Dongguan University of Technology
Lijuan Zhang
Dongguan University of Technology

Research Article

Keywords: single-pass single-layer, molten pool morphology, process parameters, multivariate regression model, neural network prediction, mathematical model

Posted Date: May 5th, 2026

DOI: https://doi.org/10.21203/rs.3.rs-9106268/v1

License: This work is licensed under a Creative Commons Attribution 4.0 International License.
Read Full License

Multi-model study on the influence of arc additive manufacturing process parameters on the morphology of the molten pool

Yuhao Zeng [a], Tinghua Ou [a], Xin Shang [a*], Lijuan Pang [b], Yansong Huang [a], Zeyu Yang [a], Dongyu Liu [a], Lijuan Zhang [a*]

a School of Mechanical Engineering, Dongguan University of Technology, Dongguan 523808, China

b Panzhihua University, Sichuan, 617067, China

[*]Xin Shang. E-mail(s): shangxin0375@126.com;

[*]Lijuan Zhang. E-mail(s): zhanglj@sdut.edu.cn;

[†]These authors contributed equally to this work.

Abstract

Wire arc additive manufacturing (WAAM) is pivotal for fabricating large-scale components, but achieving precise control over the molten pool morphology remains a challenge due to the complex coupling of process parameters. This paper systematically investigated the effects of wire feed speed (4.0–6.0 m/min) and welding speed (5–9 mm/s) on the weld bead geometry of ER120S-G high-strength steel using orthogonal experimental design. Results indicate that increasing the welding speed by 1 mm/s led to a reduction in average weld width, height and molten pool depth by 0.43 mm, 0.13 mm, and 0.08 mm, respectively. A welding speed of 6 mm/s yielded the highest process stability, with the smallest mean square errors for weld bead profile fitting (width MSE=0.0052, height MSE=0.0069). By comparing the fitting effect of four mathematical models (semi-elliptic, arc, cosine and parabola) on the contour of the weld, it was found that the semi ellipse model demonstrated superior accuracy in both single pass single-layer (average relative error 2.15%) and single pass multi-layer scenarios. Furthermore, a BP neural network model was developed, outperforming multiple linear regression with higher prediction accuracy for melt width (average error 3.24% vs. 5.4%) and melt depth (6.85% vs. 8.14%). Crucially, an optimal wire feed speed to welding speed ratio (Rsw) between 13 and 16 was identified, which

effectively suppresses defects such as humps and blow holes. This study provides a quantitative basis for optimizing WAAM process to achieve high precision forming.
Keywords: single-pass single-layer; molten pool morphology; process parameters; multivariate regression model; neural network prediction; mathematical model

1. Introduction

In the wave of global manufacturing transformation towards intelligence and lightweight, wire arc additive manufacturing (WAAM) has become a key technology for rapid manufacturing of complex components in aerospace, marine engineering and other fields due to its significant advantages of high deposition rate, low cost and high material utilization rate [1-3]. This technology accurately controls the welding speed, wire feed speed and other process parameters, realizes layer-by-layer accumulation of metal materials, breaking through the structural limitations of traditional reduction manufacturing. The accurate control of molten pool morphology is the key to achieve high-precision forming. However, due to the complex nonlinear coupling and heat accumulation effect between process parameters, the problems of unstable molten pool flow and uneven stress distribution have not been satisfactorily solved. Therefore, the existing process parameter optimization methods are difficult to meet the requirements of high-precision forming [4-7].

Domestic and foreign scholars have conducted a series of studies on the optimization of WAAM process. S·L Lawal et al. [8] systematically studied the influence of TIG/MIG welding parameters on the mechanical properties of X65 high-strength steel joints by orthogonal experimental method. They found that the coordinated optimization of welding current (180-220A) and arc voltage (28-32V) can effectively suppress the residual stress peak. Zhang et al. [9] established a cosine function prediction model based on cold metal transition (CMT) technology for the composition of protective gas (Ar/CO_2 ratio), wire feeding speed (3.5-6.5m/min), and geometric characteristics of the molten pool. They achieved accurate reconstruction of the weld width (4.2-7.8mm) under 80%Ar+20%CO_2

protection (prediction deviation <4.3%). Wan et al. [10] constructed a multivariate quadratic regression model for ultra-high frequency arc additive manufacturing by response surface methodology. They verified the prediction accuracy of the model for weld size by variance analysis (92.7% agreement). Although these linear methods offer simplicity and explicability, they are inherently difficult to capture the complex nonlinear coupling between current, voltage and wire feeding speed, which limits the accuracy and versatility of their prediction. In order to solve this problem, intelligent algorithm is introduced. Ni et al. [11] proposed a neural network model optimized by a genetic algorithm to predict weld width and residual height.

Despite these valuable contributions, there are still some limitations in the current research field. Firstly, existing models mostly focus on linear regression modeling of single-pass and single-layer process parameters, the coupling mechanism of multichannel and multilayer complex thermal physical behavior is not systematically analyzed [12]; Secondly, traditional trial-and-error methods rely on a large amount of experimental data, Although some studies have adopted advanced intelligent algorithms such as random forests[13-15] and genetic algorithms[16-18], most of them are limited to single-layer morphology prediction; Thirdly, existing process parameter optimization strategies usually only focus on one objective, making it difficult to simultaneously meet the requirements of melt pool stability and stress control. The incidence of defects such as hump and stomata is as high as 3.2% [19].

In view of the above problems, this paper takes high-strength steel ER120S-G welding wire as the research object. It analyzes the influence of welding speed (5~9mm/s) and wire feeding speed (4.0~6.0m/min) on the weld morphology through orthogonal experimental system. The BP neural network is used to construct a nonlinear mapping model between process parameters and weld width, weld height and weld depth. The semi-elliptic function is introduced to realize the high precision fitting of the multi-layer pass profile. The main innovations of this work are as follows: First, systematic multi model comparison of weld bead contour fitting; Second, customized neural network architecture provides enhanced prediction ability. This study may obtain higher prediction accuracy and stability by

constructing multiple independent output networks and performing special optimization for each morphological feature; Third, a quantitative process window (Rsw=13~16) for defect suppression is established, which provides a reliable theoretical and practical basis for optimizing WAAM process to achieve high-precision forming of complex parts.

2. Experimental Equipment

In order to meet the needs of high-strength steel arc additive manufacturing, the laboratory built a robotic arc additive manufacturing platform. System consists of a BW-2000 adjustable speed welding machine, an ABB IRB2600 six-axis industrial robot (arm length 1.58m, end load 10kg) and an L-type positioner. The L-type positioner has ±90° flip and 360° rotation functions, the workbench is equipped with 6 sets of fixtures, they suppress thermal deformation of the substrate, they cooperate with the robot to achieve full-position additive manufacturing.

Q235 steel plate is selected as the substrate. its size is 200mm*200mm*20mm, the welding wire material is ER120S-G, its chemical composition is shown in Table 1. The diameter of the welding wire is 1.2mm, the shielding gas is 80%Ar+20%CO2, the gas flow rate is 22L/min, the welding wire extension length is 15mm, the welding voltage is 22V. The spatter is controlled by keeping the height of the welding wire end constant, the middle section of the sample is cut by electric spark wire cutting. After polishing, the cross-sectional morphology of the weld is observed using a microscope.

Tab.1 ER120S-G Chemical chemistry

C	Mn	Si	P	S	Ni	Cr	Mo	V	Ti	Zr	Al	Cu
0.09	1.90	0.80	0.005	0.005	2.15	0.35	0.55	0.004	0.08	0.012	0.01	0.13

3. Analysis of Single-Channel Single-Layer Size and Process Parameters

In arc additive manufacturing, the forming quality of a single-pass single-layer weld

directly affects the dimensional accuracy and structural stability of the multi-layer stacking process, its cross-sectional morphology characteristics play a decisive role in the overall forming quality. Carrying out weld dimensional morphology prediction and analysis can effectively reduce the subsequent machining material loss, it is especially important for the lightweight manufacturing of complex structural parts. The typical cross-sectional morphology is shown in Figure 1.



Fig.1 weld section morphology

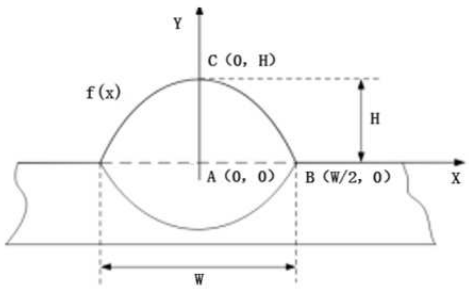


Fig. 2 weld section model

As shown in Figure 2, assuming that the cross section of the weld is symmetrically distributed, the distance between 2AB is defined as the weld width, point C is the highest point of the weld bead. Since the welding speed (WS) and wire feeding speed (WFS) have the most prominent influence on the geometric dimensions of the weld, When WS<5mm/s, the molten pool overheats and collapses, and when WS>9mm/s, the metal supply is insufficient and the weld is broken; The molten depth is not enough when WFS<4.0m/min, and the welding wire is not fully melted when WFS>6.0m/min. Therefore, in this study, the welding speed is in the range of 5-9 mm/s, the wire feeding speed is in the range of 4.0-6.0 m/min to carry out the printing test. The specific test parameters are shown in Table 2.

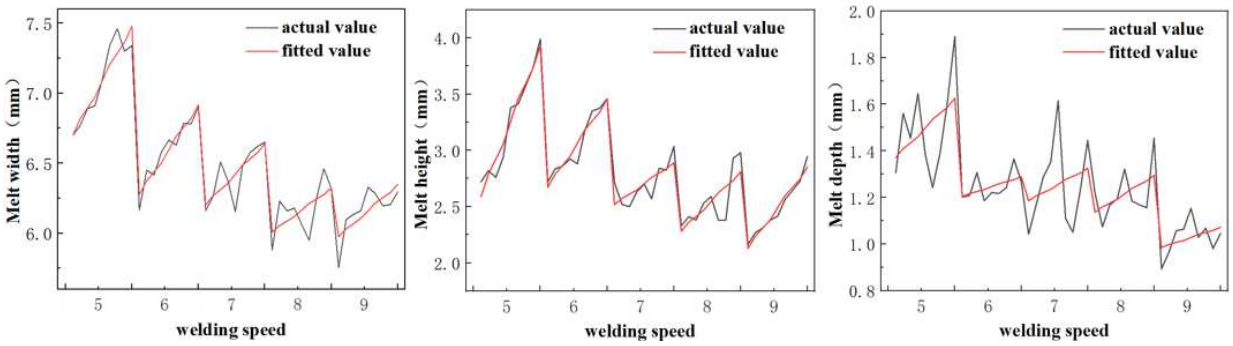
Tab.2 Process Scheme Parameters

Serial number	Welding speed (mm/s)	Wire feeding speed (m/min)	Weld High (mm)	Weld Width (mm)	Molten pool Depth (mm)
1	5	4.0	2.723	6.703	1.306
2	5	4.5	2.761	6.890	1.454
3	5	4.7	2.942	6.910	1.646
4	5	5.0	3.379	7.102	1.384

5	5	5.5	3.565	7.460	1.392
6	5	5.7	3.732	7.301	1.610
7	5	6.0	3.987	7.340	1.890
8	6	4.0	2.723	6.165	1.202
9	6	4.5	2.861	6.415	1.307
10	6	4.7	2.925	6.58	1.185
11	6	5.0	2.88	6.665	1.222
12	6	5.5	3.35	6.785	1.243
13	6	5.7	3.375	6.78	1.365
14	6	6.0	3.46	6.9	1.270
15	7	4.0	2.715	6.16	1.042
16	7	4.5	2.5	6.51	1.289
17	7	4.7	2.63	6.375	1.352
18	7	5.0	2.7	6.155	1.615
19	7	5.5	2.84	6.575	1.051
20	7	5.7	2.825	6.62	1.232
21	7	6.0	3.035	6.65	1.444
22	8	4.0	2.33	5.88	1.218
23	8	4.5	2.38	6.16	1.168
24	8	4.7	2.527	6.180	1.193
25	8	5.0	2.586	6.062	1.322
26	8	5.5	2.382	6.251	1.169
27	8	5.7	2.934	6.463	1.156
28	8	6.0	2.983	6.322	1.454
29	9	4.0	2.169	5.755	0.894
30	9	4.5	2.312	6.135	1.058
31	9	4.7	2.384	6.162	1.064
32	9	5.0	2.421	6.331	1.154
33	9	5.5	2.653	6.195	1.068
34	9	5.7	2.750	6.205	0.981
35	9	6.0	2.954	6.295	1.045

After measuring the single-pass single-layer cross section by combining vernier

calipers with microscope measurements, MATLAB software is used to mathematically model the cladding layer and width, the fitting curves of the cladding height and width and the cladding process parameters (wire feeding speed, welding speed) are obtained. At the same time, the fitting significance and stability of the model are checked, as shown in Figure 3:



(a) Weld width (b) Weld height (c) Molten pool depth

Fig. 3 Fitting of cladding process parameters to the surface size of high strength steel

As shown in Figure 3, the line graph is divided into five intervals, each representing a different welding speed. It can be clearly observed from the figure that with the increase of welding speed, the weld width, weld height and molten pool depth all show a trend of gradually decreasing. When the welding speed increases, the melting amount of the welding wire cannot keep pace with the moving speed of the molten pool, resulting in a decrease in the metal supply per unit length of the weld, the weld height is reduced significantly. It can be seen that when the speed increases from 6mm/s to 9mm/s, the weld height drops from 2.72mm to 2.17mm. At the same time, the weld width is reduced because of the liquid metal cannot be fully spread, the molten pool depth becomes shallower due to the dilution effect of heat input.

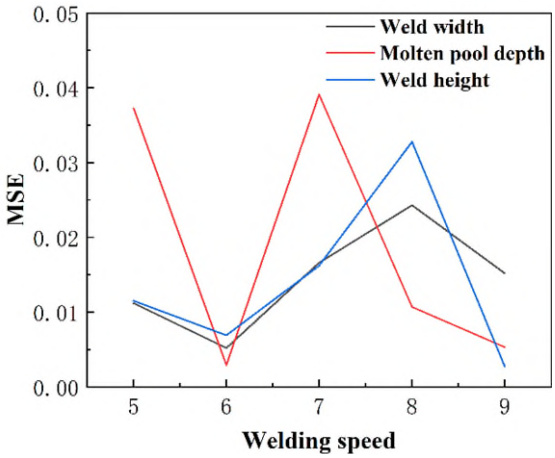


Fig. 4 Mean square error of different welding speeds

As shown in Figure 4, the mean square error (MSE) is used as the evaluation indicator. MSE is a common method to measure the difference between the predicted value and the actual observed value. It quantifies the prediction accuracy of the model by calculating the average of the squared values of the prediction errors. Specifically, the closer the MSE value is to 0, the higher the fitting accuracy of the selected process parameters to the weld bead profile, the smaller the deviation between the predicted value and the actual observed value. The analysis results show that compared with other process parameters, the welding speed of 6mm/s shows higher stability and better fitting effect. On this basis, the regression equation of the optimized welding speed and wire feeding speed on the weld bead profile is obtained, it specifically describes the quantitative relationship between the two.

$$\text{Weld height: } H = 0.1833X_1 + 0.3929X_2 \quad (1)$$

$$\text{Weld width: } W = 0.8340X_1 + 0.3929X_2 \quad (2)$$

$$\text{Molten pool depth: } Y = 0.0723X_1 + 0.1929X_2 \quad (3)$$

In the formula: X_1 is the welding speed, mm/s; X_2 is the wire feeding speed, m/min.

The fitting degree of the weld height, weld width and molten pool depth obtained from MATLAB is 0.0069, 0.0052 and 0.0029, it shows that the model fits well and the welding speed of 6mm/s is relatively stable.

3.1. Error Analysis of Regression Results

In order to further verify the regression accuracy of the process parameters, all

parameters are selected for verification at a welding speed of 6 mm/s. The process parameter data are substituted into the above regression equation to obtain the single-pass single-layer weld width W, weld height H and molten pool depth Y predicted by multiple regression, then compared with the experimental results. The error calculation formula is:

$$e = \frac{|A_2 - A_1|}{A_2} \times 100\% \tag{4}$$

In the formula: e is the error rate, A_1 is the predicted value, and A_2 is the experimental value. The average error rate is the mean of the absolute values of each error rate.

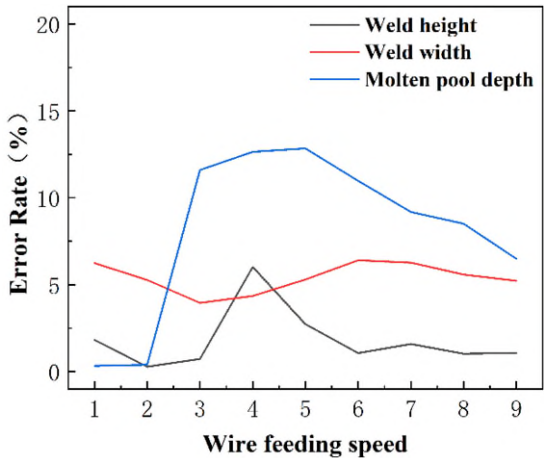


Fig.5 Error values of different process parameters for welding speed 6mm/s

As shown in Figure 5, the multivariate regression model is more accurate in predicting the weld height, the error rate of the prediction results under different process parameters does not fluctuate much, with an average error rate of 1.82%. However, the weld width and molten pool depth fluctuate greatly under different process parameters, they are 5.4% and 8.14% respectively.

In order to further improve the prediction accuracy, the study found that it is difficult to fully describe the material forming process by relying only on the two process parameters of welding speed and wire feeding speed. Since process parameters such as current and voltage have a significant impact on weld bead formation, there is a complex nonlinear coupling relationship between the parameters, the traditional linear regression model is difficult to accurately reveal the intrinsic relationship between additive manufacturing process parameters and weld bead morphology characteristics. In view of this, the study introduces a neural network model for in-depth analysis to fully explore the nonlinear mapping law under

the interaction of multiple parameters.

3.2. Basic Principles of Neural Networks

The artificial neural network model shown in Figure 6 includes the input layer, the hidden layer and the output layer, and each layer is composed of neuron nodes.

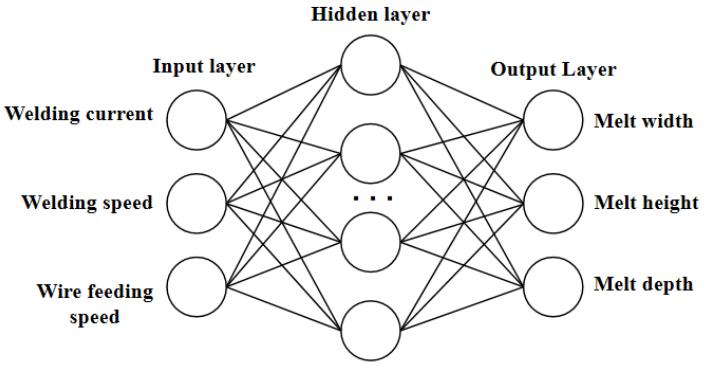


Fig.6 Neural network structure diagram

In the design of neural network architecture, the number of hidden layers and the number of neurons is the core factors, they affect the prediction accuracy. Since this paper focuses on the influence of the four process parameters of welding speed, wire feeding speed, current and voltage on the three result indicators of weld width, weld height and molten pool depth. After research, it is found that the influence of welding voltage on the three indicators of weld width, weld height and molten pool depth is not obvious, so the final input parameters are determined to be welding speed, wire feeding speed and current, the output result indicators are still weld width, weld height and molten pool depth. Based on such parameter determination, a neural network with 3 inputs and 3 outputs can be constructed, it can realize the prediction of weld width, weld height and molten pool depth at one time.

However, according to the basic principles of neural networks, neural networks with multiple outputs often have a certain degree of reduction in prediction accuracy, so three neural networks with a structure of 3 inputs and 1 output are constructed. These three neural networks focus on the three indicators of weld width, weld height and molten pool depth to carry out predictions, so as to achieve more accurate and effective predictions of each

indicator, it is decided to set only one hidden layer. The number of neurons in the hidden layer m can be determined according to the empirical formula [20].

$$m = \sqrt{A + B} + C \tag{5}$$

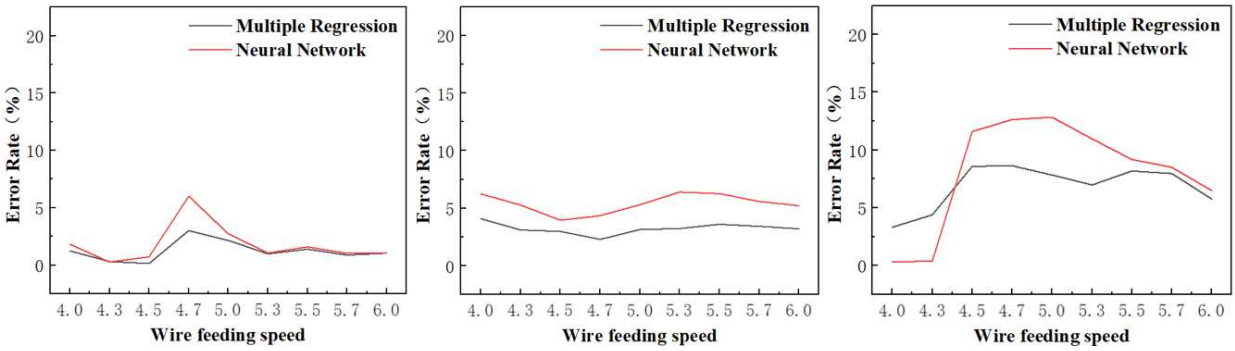
In the formula: A is the number of neurons in the input layer, B is the number of neurons in the output layer, C is a constant between 0 and 10. In the specific calculation, the value of C is a decision-making process that requires comprehensive consideration of multiple factors. In practice, several different C values are usually tried, techniques such as cross-validation are used to evaluate the performance of different models, thus the best C value is selected.

After determining the structure of the neural network, all parameters in welding speed 6 are selected for verification, the process parameter data is substituted into the training to obtain the predicted values of weld width, weld height, and molten pool depth. Since the initial weight values of each neuron in the neural network are random, the training results of each neural network are different, so multiple trainings are performed, then calculate each training to get the performance index of the mean and standard deviation. This method can provide a more robust performance evaluation, it helps identify the variability of model performance.

3.3. Molten Pool Morphology Analysis Based on Neural Network and Multivariate Regression Model

Through multiple rounds of training, it is found that the results fluctuated due to the randomness of the initial weights of the neural network. To ensure the generalization ability of the model, multiple sets of training results are screened based on indicators such as the average error of the validation set. The average prediction errors of the optimized neural network for weld height, weld width and molten pool depth are 1.24%, 3.24% and 6.85% respectively. Compared with the multivariate regression model, the prediction accuracy of weld width and molten pool depth increased by 2.16% and 1.29% respectively. The comparison results are shown in Figure 7, verifying the prediction advantage of neural

networks in nonlinear complex systems.



(a)weld height (b) weld width (c) Molten pool depth

Fig.7 Comparison of error rate of prediction results

In the field of additive manufacturing, the neural network method has shown significant advantages in the prediction of single-pass forming morphology: its powerful nonlinear mapping ability can effectively capture the complex coupling relationship between process parameters, the prediction accuracy increases exponentially with the increase of training data. Compared with the traditional linear regression model, this method supports multi-parameter input (such as welding current, voltage, etc.), breaking through the limitations of single factor analysis. In actual production, the initial prediction model can be constructed based on some experimental data, continuous optimization can be achieved through incremental learning, ultimately realizing intelligent selection of process parameters and closed-loop control of forming quality.

4. Modeling of Single-Track Single-Layer Cross-Section Size and Contour of High-Strength Steel

In order to further explain the rationality of selecting a welding speed of 6 mm/s, domestic and foreign researchers have accumulated experience in mathematical modeling and analysis in recent years. In the fitting of single-pass single-layer surface profiles, mathematical models such as arcs, semi-ellipses, parabolas, and sine (or cosine) have been

used. These models are of great significance for optimizing the performance of high-strength steel. [21-22] On this basis, combined with their own experimental data and MATLAB mathematical modeling tools, the parameters of these mathematical models are optimized to determine an optimal parameter selection range. The specific mathematical functions and their expressions are shown in Table 3 below.

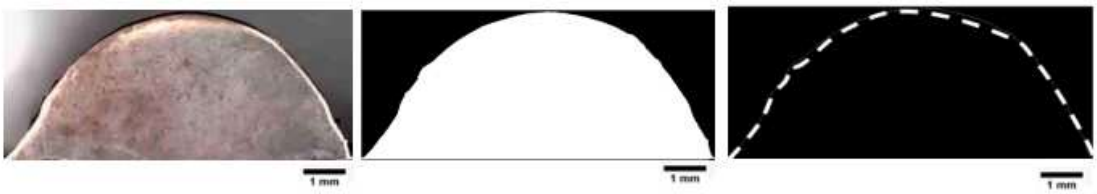
Tab.3 The single-channel single-layer profile mathematical model[23]

Model	Model Function	Weld bead cross-sectional predicted area Ap/mm2
Arc Model	$y = a + \sqrt{b^2 - x^2}\,(a < 0, b > 0)$	$A_1 = \int_{-w/2}^{w/2} (a + \sqrt{b^2 - x^2})$
Semi-ellipse model	$y = a + \sqrt{b^2 - \frac{b^2 x^2}{c^2}}\,(a \le 0, b > 0, c > 0)$	$A_2 = \int_{-w/2}^{w/2} (a + \sqrt{b^2 - \frac{b^2 x^2}{c^2}})$
Cosine Model	$y = a + b\cos(cx)(a \le 0, b > 0, c > 0)$	$A_3 = \int_{-w/2}^{w/2} (a + b\cos(cx))$
Parabolic Model	$y = ax^2 + b(a < 0)$	$A_4 = \int_{-w/2}^{w/2} (ax^2 + b)$

Combined with the mathematical model of single-pass single-layer contour in Table 3, the parameters are fitted and optimized. First, the color image is converted into a grayscale image (0-255 grayscale), the Otsu adaptive threshold method is used to achieve binary segmentation: the grayscale value is compared with the threshold pixel by pixel, the grayscale value is set to white (255) if it is greater than the threshold, otherwise it is set to black (0), to ensure accurate segmentation of the weld area. In this way, the cross-section area of the bead in the image can be rendered white, the rest is set to black, thereby ensuring the accuracy of the weld cross-sectional extraction results, as shown in Figure 8a-b. In order to enhance edge continuity, the Canny algorithm is introduced to form a complete contour line (Figure 8c).

Then, the bwboundaries function is used to extract the contour coordinates, the infill function is combined to fill the internal holes. The region props function is used to calculate the actual cross-sectional area A_0. The least squares method is used to fit the semi-ellipse, arc,

cosine function and parabola. In the process of semi-ellipse fitting, the upper half of the ellipse equation is defined as the fitting function, it covers the specific parameters such as the ellipse center coordinates, major axis length, minor axis length and rotation angle; arc fitting constructed a circle equation fragment, including the center, radius and angle parameters; when fitting the cosine function, the amplitude, frequency and phase and other related parameters are set; for parabola fitting, it is based on the standard equation of the parabola, specific parameters such as vertex coordinates, opening direction and opening width are introduced. In these fitting scenarios, the lsqnonlin function of MATLAB is used to minimize the sum of square errors between the actual contour points and the corresponding points of the fitting curve through an iterative optimization process, so as to determine the optimal fitting parameters. Then, a fitting curve is constructed based on these parameters, the area under the curve is calculated, the result is used as an accurate approximation of the cross-sectional area of the weld bead.



(a) Original Image (b) Binarization Processing (c) Canny Edge Detection

Fig.8 Picture processing process

4.1 Fitting Results

In order to further study the correlation, the MATLAB fitting program is used to analyze the weld cross section under each set of welding parameters. The statistical results are shown in Table 4, the relative error e between the bead area predicted by the model and the bead area obtained by calculation, its expression can be expressed as:

$$e = \frac{|A_p - A_0|}{A_0} \times 100\% \quad (6)$$

In the formula: A_0 is the actual area of the weld cross section, it can be regarded as the experimental measurement value. A_p, namely A_1, A_2, A_3, A_4, is the cross-sectional area of

the weld obtained by the mathematical model.

Tab.4 The adaptive fitting results of the four model functions

Test serial number	Welding Speed V_w/(mm·s^{-1})	Wire Feeding Speed V_S/(m·min^{-1})	Weld width W/mm	Weld height h/mm	Calculate area A_0/mm^2	Parabolic model		Cosine model		Circle model		Semi-elliptical model	
						SEM	A_1/mm^2	SEM	A_2/mm^2	SEM	A_3/mm^2	SEM	A_4/mm^2
1	5	3.7	6.372	2.865	13.951	77.534	12.868	69.134	12.986	80.307	12.830	56.055	13.168
2	5	4.7	6.911	2.943	17.719	64.242	16.582	60.087	16.655	72.349	16.438	48.746	16.856
3	5	5.7	7.312	3.728	21.492	60.81	20.183	59.12	20.220	70.005	19.986	50.043	20.415
4	6	3.7	6.169	2.865	11.624	68.209	10.827	64.969	10.865	84.629	10.637	48.948	11.051
5	6	4.7	6.578	2.925	14.767	61.908	13.856	60.114	13.882	80.311	13.584	43.641	14.125
6	6	5.7	6.782	3.375	17.913	76.197	16.545	71.959	16.621	94.117	16.224	47.529	17.059
7	6	6.7	7.425	3.574	21.052	84.145	19.279	82.577	19.312	97.362	19.001	60.146	19.784
8	7	3.7	5.903	2.675	9.957	81.078	9.152	84.644	9.117	98.202	8.982	74.644	9.217
9	7	4.7	6.375	2.632	12.661	70.188	11.771	61.722	11.879	86.215	11.569	71.722	11.752
10	7	5.7	6.622	2.825	15.353	61.217	14.410	57.957	14.460	94.47	13.900	67.957	14.307
11	7	6.7	7.031	3.155	18.044	76.404	16.662	70.733	16.764	90.953	16.399	68.733	16.800
12	8	3.7	5.792	2.771	8.723	55.416	8.237	52.324	8.264	88.893	7.945	62.324	8.177
13	8	4.7	6.183	2.529	11.074	43.124	10.593	42.184	10.603	77.157	10.216	73.184	10.260
14	8	5.7	6.462	2.927	13.432	58.928	12.639	56.903	12.666	88.231	12.245	79.903	12.357
15	9	3.7	5.625	2.763	7.748	67.005	7.231	60.283	7.283	95.25	7.012	80.283	7.128
16	9	4.7	6.163	2.382	9.843	92.916	8.926	91.824	8.936	109.307	8.764	99.916	8.857
17	9	5.7	6.205	2.725	11.941	118.201	10.529	118.04	10.531	125.104	10.446	112.831	10.593
18	9	6.7	6.755	3.085	14.034	135.427	12.130	134.466	12.143	138.675	12.084	137.257	12.104

The experimental results show that there is a significant difference between the theoretical cross-sectional area (A_0) calculated based on the volume of deposited material per unit length and the area predicted by the model (A_p). Among them, A_p is obtained by fitting four mathematical models: A_1 is a parabola model, A_2 is a cosine model, A_3 is an arc model, A_4 is a semi-ellipse model. Through the relative error formula analysis, it is found that the e-values of each model are less than 8.5% (Table 4), but the difference in e-values between different models is small (for example, the difference in e-values between A 4 and A 1 is only 0.73%). Therefore, it is more statistically significant to use the mean square error (MSE) as a quantitative evaluation indicator - this index is calculated by calculating the mean square deviation of the predicted value and the theoretical value, it can effectively distinguish the difference in fitting accuracy of the model at the edge of the molten pool, the optimal parameter combination is selected.

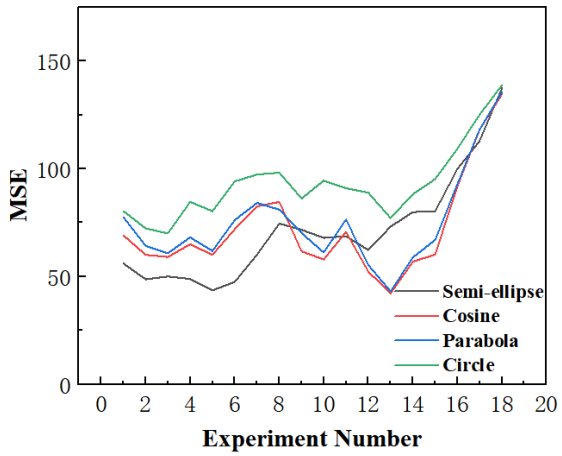
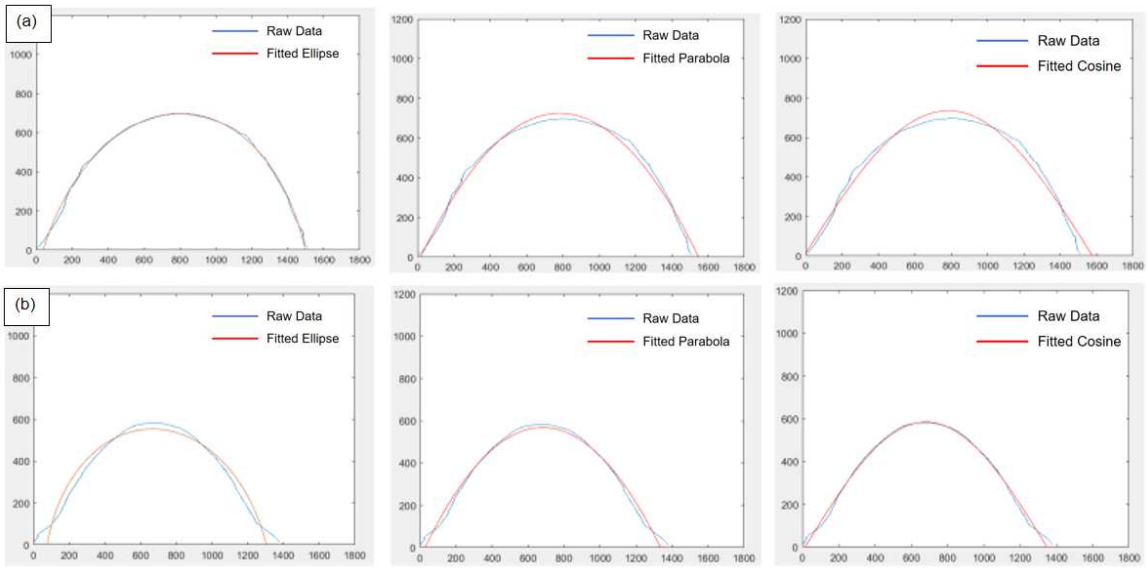


Fig.9 Relative differences between predicted and actual values

As shown in Figure 9, when the welding speed is in the range of 5-8 mm/s, the semi-ellipse model has the highest fitting accuracy for the weld cross section (average MSE = 48.75). As the welding speed further increases to 9 mm/s, the weld cross section shows obvious flattening characteristics (the ratio of weld width/weld height increases from 2.35 to 2.64), the fitting accuracy of parabolic model and cosine model is improved significantly (Figure 10b).



(a) welding speed 6 mm/s (b) welding speed 9 mm/s

Fig.10 Lane cross-section analysis results obtained using the fitting procedure

4.2 Optimal Model Function

In order to further visualize the relationship between wire feeding speed and welding speed, thus better select the fitting parameters, from Figure 11, at low wire feed speed to welding speed ratio, the cosine model and parabola model have higher goodness of fit to the cross-section profile of single pass [24]. It can be seen that when the wire feeding speed is at a relatively low level and the welding speed is at a relatively high level, the geometric shape of the cross-sectional profile of the weld bead may be closer to a cosine curve or parabola.

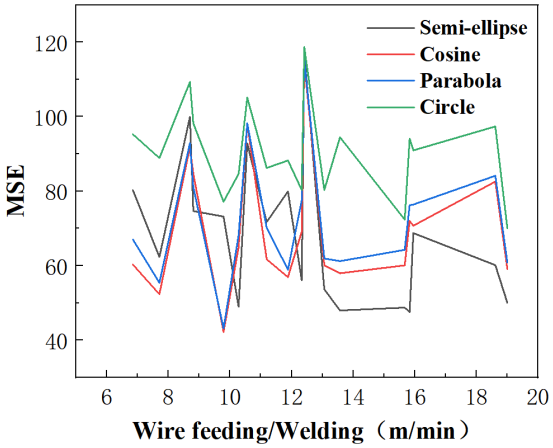


Fig.11 Relations of MSE values for different models in the ratio of Rsw

As the welding speed increases, the Rsw value gradually decreases. When it is less than

12, the cosine fit is better than other fitting models. For example, No. 15 in Table 4: WS = 9 mm/s, WFS = 3.7 m/min, Rsw = 6.85, the SEM value of the semi-ellipse model is 80.283, it is 24.9% lower than the 60.283 of the cosine models. The molten pool volume is only 7.75 mm^3. Liquid metal is more likely to form a gentle cosine-shaped profile under the action of surface tension, but at the same time, the supply of molten metal is also reduced accordingly, it makes the molten metal solidify rapidly, then cuts off the molten pool, finally forms a discontinuous weld. The exact experimental results show that in the process of carrying out a single-pass multi-layer cladding experiment, the surface of the weldment is uneven as shown in Figure 12.



Fig.12 Single-pass multi-layer cladding at a welding speed of 9 mm/s

In contrast, when Rsw>16, such as WS=5mm/s, WFS=5.7m/min, Rsw=19 in No. 3, the SEM value of the semi-ellipse model is 50.043, it is 15.4% lower than the 59.12 of the cosine models, the molten pool volume expands to 21.49mm^3. The liquid metal presents a semi-ellipse shape under the coupling of gravity and surface tension, but the wire feeding speed is too fast, resulting in the failure of the welding wire to fully melt, it leads to an unstable state in the droplet transition process as shown in Figure 13. This unstable state may cause the molten droplet to produce violent impact and vibration when it contacts the molten pool, thereby forming spots on the weld surface. As shown in Figure 14, the heat is concentrated at the spots and cools rapidly, making it difficult for the gas in the molten pool to fully escape in a short time, thereby forming pores. In addition, this special thermal process makes it very easy for the cladding layer to produce large residual stress and thermal stress, the accumulation of these stresses may eventually cause the formation of cracks.

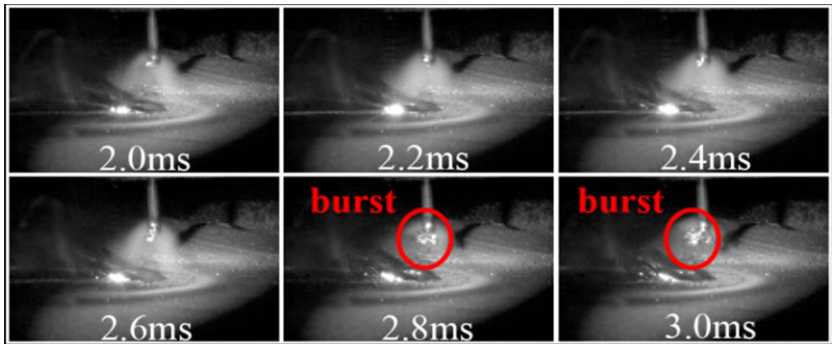


Fig.13 The process of forming the spots



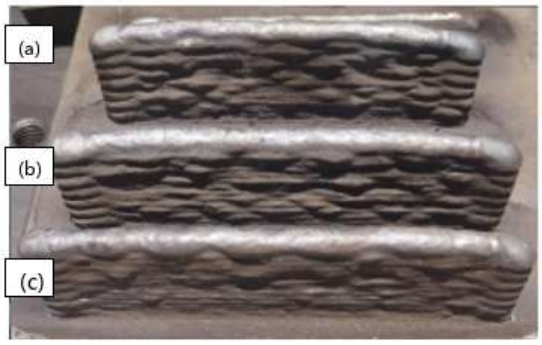
Fig.14 Spots appearing too high at Rsw

Therefore, the optimal wire feeding/welding ratio (Rsw) is between 13 and 16. Taking the data of test No. 5 as an example, when the welding speed (WS) is 6mm/s and the wire feeding speed (WFS) is 4.7m/min, the Rsw value is 13.05. Under this parameter, the semi-elliptical model (SEM) value is 43.641, it is 27.4% lower than the 60.114 of the cosine models; at the same time, the molten pool volume is 14.77mm³, the liquid metal presents a semi-elliptical shape under the combined action of gravity and surface tension. When the welding parameters within this range are used for stacking operations, the wire feeding speed and the welding speed reach a relatively ideal balance state, it can effectively promote the full mixing and uniform distribution of the molten metal in the molten pool, thereby reducing the common spatter phenomenon during welding, enhancing the stability of the arc.

5.Single-Channel Multi-Layer Modeling

5.1. Preparation of Single-Layer Multilayer

In order to verify whether the optimal Rsw parameter of a single pass and a single layer is accurate, the parameters within and outside the range are selected for experiments, the cross-sectional profile is modeled. The cross-sectional profile and size of the weld under different process parameters can be predicted through modeling, providing a reliable basis for the optimization of process parameters. The three groups of parameters in Figure 15 are printed to study the process parameters.



(a) WS = 7 mm/s, WFS = 4.7 m/min (b) WS = 5 mm/s, WFS = 4.7 m/min (c) WS = 6 mm/s, WFS = 4.7 m/min

Fig.15 Preparation of single-channel multilayers

The experiment uses wire cutting to process the cross section of a single multilayer deposit. After grinding, polishing and corrosion treatments, the result is shown in Figure 16. The weld bead profile, interlayer bonding state and dimensional parameters are observed and recorded through a metallographic microscope (50-200×). During the process implementation, the interlayer cooling to room temperature is strictly controlled before reciprocating deposition, it effectively reduces the height difference between the arc starting and arc extinction points, finally, the stable forming data under three typical working conditions are obtained.



Fig.16 Cross section of the microscope

5.2. Single-Channel Multi-Layer Cross-Section Profile Acquisition

Since remelting is inevitable in the process of single-pass multi-layer deposition, the observed cross-sectional images are processed and analyzed by MATLAB. Through grayscale, binarization, edge detection and other image processing technology, the contour curve of each bead can be extracted, calculating the cross-sectional area of the actual weld bead. These contour curves and cross-sectional area data can be used to evaluate the quality of cladding, optimize process parameters and establish mathematical models. The contour of each layer is calculated by combining the area estimation method [25-26]. The calculation principle is shown in Figure 17.

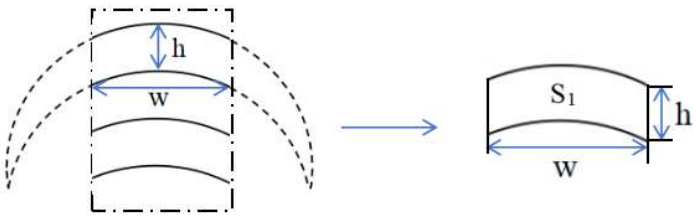


Fig.17 Count on each layer by using the area estimation method

The extracted weld bead contour curve is combined with the area estimation method, the actual area is calculated using the formula, the mathematical model is fitted to the weld bead.

$$A_p = \int_{-w/2}^{w/2} f(x)\,dx \tag{7}$$

$$S_1 = hW \tag{8}$$

$$h = \frac{\int_{-w/2}^{w/2} f(x)\,dx}{w} \tag{9}$$

In the formula, A_p is the cross-sectional area of a single channel and a single layer, S_1 is the cross-sectional area of each layer, $f(x)$ is a single-channel single-layer cross-section profile curve, h is the lifting amount, W is the width of a single pass and a single layer. Thus, the weld bead can be calculated.

Tab.5 Adaptive fitting results of the three model functions

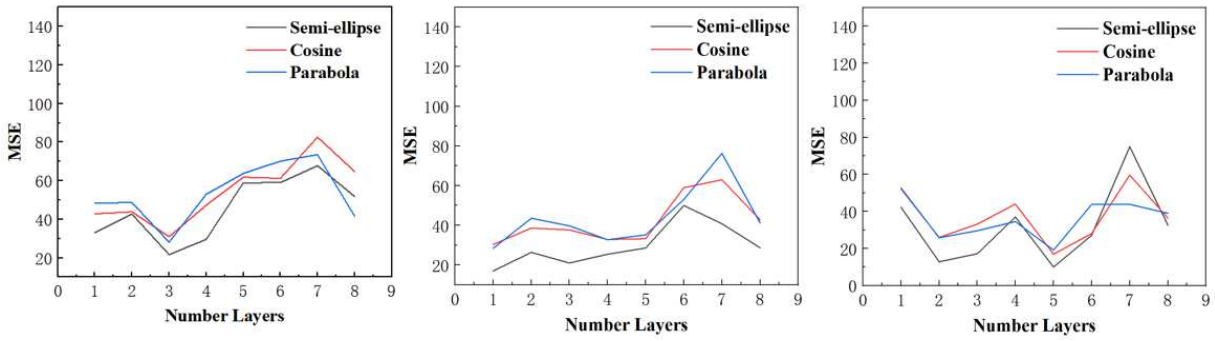
Test serial number	Welding Speed V_w/(mm·s^{-1})	Wire Feeding Speed V_S/(m·min^{-1})	Weld width W/mm	Weld height h/mm	Calculate area A_0/mm^2	Parabolic model		Circle model		Semi-elliptical model	
						SEM	A_1/mm^2	SEM	A_2/mm^2	SEM	A_3/mm^2
1	5	4.7	6.91	2.94	17.72	64.24	16.58	60.09	16.66	48.75	16.86
2	5	4.7	6.99	5.31	32.24	48.68	30.67	43.89	30.83	48.75	30.67
3	5	4.7	7.00	7.43	52.01	28.15	50.55	30.98	50.40	21.69	50.88
4	5	4.7	7.00	9.74	68.18	53.00	64.57	47.26	64.96	29.59	66.16
5	5	4.7	7.00	11.68	81.76	63.76	76.55	61.85	76.70	58.95	76.94
6	5	4.7	7.01	13.81	96.59	70.18	89.81	61.27	90.67	59.05	90.89
7	5	4.7	7.03	16.46	115.62	41.62	110.81	64.75	108.13	51.78	109.63
8	5	4.7	7.04	19.12	134.53	113.49	119.26	122.62	118.03	107.81	120.03
9	6	4.7	6.58	2.93	14.71	28.33	14.29	30.34	14.26	16.99	14.13
10	6	4.7	6.66	5.28	26.76	43.55	25.60	38.59	25.73	26.36	26.06
11	6	4.7	6.66	7.40	43.18	39.75	41.46	37.69	41.55	21.00	42.27
12	6	4.7	6.67	9.69	56.60	32.75	54.74	32.87	54.74	25.41	55.16
13	6	4.7	6.67	11.63	67.87	35.21	65.48	33.21	65.62	28.56	65.93
14	6	4.7	6.68	13.74	80.18	53.05	75.93	58.96	75.45	49.98	76.18
15	6	4.7	6.70	16.38	95.98	41.22	92.02	42.82	91.87	28.69	93.23
16	6	4.7	6.70	19.02	111.68	116.28	98.69	102.97	100.18	80.82	102.65
17	7	4.7	6.38	2.63	12.66	52.67	11.99	52.16	12.00	42.27	12.12
18	7	4.7	6.45	4.75	23.03	25.79	22.44	25.97	22.44	12.88	22.74

19	7	4.7	6.45	6.65	37.16	29.64	36.06	33.17	35.93	17.18	36.52
20	7	4.7	6.46	8.71	48.71	34.54	47.03	44.03	46.57	37.03	46.91
21	7	4.7	6.46	10.45	58.41	19.14	57.30	16.92	57.43	10.03	57.83
22	7	4.7	6.47	12.35	69.01	43.77	65.99	28.09	67.07	27.11	67.14
23	7	4.7	6.49	14.73	82.60	39.00	79.38	36.40	79.60	32.65	79.91
24	7	4.7	6.49	17.10	96.11	83.86	88.05	99.62	86.54	114.91	85.07

In arc additive manufacturing, as the number of deposited layers increases, the printing process has a significant impact on the melting and solidification of the current cladding layer, it is mainly reflected in heat conduction. Specifically, the temperature of the previous layer affects the heating and cooling rate of the current layer. Due to gravity and surface tension, the molten pool can flow toward the solidified previous layer, thereby changing the final shape of the weld. Affected by these thermal effects and physical phenomena, the cross-sectional profile of the weld is irregular, so it is not appropriate to use circular fitting when depositing [27].

5.3. The Best Model Function at Different Layers

As shown in Table 5, the experimental data of welding speed = 5-7mm/s, the wire feeding speed = 4.7m/min (Figure 18): The SEM of the first layer semi-ellipse model at welding speed = 6mm/s (serial number 9) is 43.64, it is 22.1% and 41.5% higher than that of welding speed = 5mm/s and welding speed 7, respectively, it is highly consistent with the experimental observation; with the increase of the number of layers, the fitting effect of welding speed 7 (SEM decreased from 84.64 to 61.72) and parabola model (SEM decreased from 98.20 to 70.18) is improved, but the semi-ellipse model still maintains the lowest SEM value (43.77), it is 34% lower than the cosine model; when the number of layers exceeds 5, the weld width increases by 15% and the weld height decreases by 8%, the SEM value of the 8th layer (59.05) is 48.6% and 49.2% lower than that of welding speed 5mm/s (114.91) and welding speed 7mm/s (116.28), respectively. In general, for the second and higher layers of weld bead contours, the semi-ellipse model function shows the highest fitting accuracy. Under the combined effect of these factors, the metal liquid in the molten pool flows more to both sides under the influence of gravity, resulting in a decrease in layer height and a corresponding increase in weld width, making the shape of the weld bead closer to an ellipse. When the number of stacked layers increases further, the shape change of the molten pool gradually stabilizes, forming a relatively stable contour shape.



(a)V_w=5.0mm/s V_s=4.7m/min (b)V_w=6.0mm/s V_s=4.7m/min (c)V_w=7.0mm/s V_s=4.7m/min

Fig. 18 layers and SEM of each model

6.Conclusions

This study focuses on the single-pass single-layer printing process of arc additive manufacturing technology. Through systematic experiments and mathematical modeling analysis, the influence mechanism of key process parameters on morphological characteristics such as weld width, weld height and molten pool depth is deeply explored. The study uses high-strength steel as the experimental material, using the built arc additive manufacturing system, by adjusting welding speed and wire feed speed and other process parameters, the influence of these factors on the cross-section morphology of weld bead is analyzed systematically

(1) Experimental results show that with the increase of welding speed, the weld width, weld height and molten pool depth all show a downward trend. By comparing the application effects of various mathematical models in weld cross-sectional profile fitting, this study finds that the semi-elliptic function shows the best performance in single-layer single-pass and single-pass multi-layer welding cross-sectional profile fitting. This discovery provides theoretical support and practical guidance for optimizing arc additive manufacturing process parameters, it improves the quality and stability of formed parts.

(2) The weld width, weld height and molten pool depth are predicted by using a multiple regression model and a neural network model. The results show that the neural network model has higher prediction accuracy than the multiple regression model, especially

for the prediction of weld width and molten pool depth. This is due to the highly nonlinear function approximation ability, adaptive learning ability and fault tolerance of the neural network model, so that it can reflect the complex relationship between the process parameters and the morphology of the weld pipe more accurately.

(3) The cross-sectional morphology of a single-pass multilayer deposit is analyzed and evaluated by cross-sectional profile modeling and image processing technology. The experimental results show that during the depositing process, the cross-sectional profile of the weld is often affected by multiple factors, such as heat conduction and molten pool flow behavior, resulting in the shape profile not being a regular circle. By comparing the fitting effects of different model functions, in this study, it is found that the semi-elliptic model function shows the highest fitting accuracy in the high number of bead contour fitting.

This article reveals the influence mechanism of arc additive manufacturing process parameters on weld bead morphology, it also provides effective methods and theoretical support for optimizing process parameters and improving the quality and stability of formed parts. The parameter window of Rsw=13-16 in this study, when applied to the WAAM of ER120S-G steel components on a large offshore platform, can reduce the hump defect rate from 3.2% to 0.5% and decrease the machining allowance by 18%. In the future, with the continuous development and widespread application of arc additive manufacturing technology will provide important reference and reference for its further development and application.

Statements and Declarations

Funding

We would like to express their gratitude for the financial support received from the Guangdong Major Project of Basic and Applied Basic Research Foundation (No. 2020B0301030001). This work was also supported by the opening project of the State Key Laboratory of Explosion Science and Technology (Beijing Institute of Technology, KFJJ23-21M), the grants from the Guangdong Basic and Applied Basic Research Foundation (Grant numbers[2022A1515010933.]and [2023A1515240084.]), and the Key Fields Special Project for High-end Equipment Manufacturing (Intelligent Robotics, New

Materials) funded by the Guangdong Provincial Department of Education (Approval number: 2024ZDZX3014).

Competing Interests

The author has no relevant financial or non-financial interests to disclose.

Data Availability Statement

The authors do not have permission to share data.

Author Contributions

All authors contributed to the conceptualization and design of the study. Yuhao Zeng: methodology, investigation, data curation, visualization, writing—original draft. Tinghua Ou: validation, formal analysis, data curation, revise the article. Xin Shang: funding acquisition, supervision, writing, review, and editing. Lijuan Pang: Material preparation, data collection and analysis. Yansong Huang: conceptualization, formal analysis, data curation. Zeyu Yang: validation, formal analysis, data curation. Dongyu Liu: data organization, data bureau analysis.

References

[1] Lu Bingheng. Intelligent Manufacturing and Additive Manufacturing[J]. Science and Technology Association Forum, 2016 (10): 11-12.

[2] Huang Weidong. Research progress of material 3D printing technology[J]. New Industrialization, 2016, 6 (3): 53-70.

[3] Zhang J, Yang M, Zhao X, et al. Microstructure and mechanical properties of Ti6Al4V-(TiC+TiB)/Ti laminated composites fabricated by hot press plus hot rolling[J]. Journal of Alloys and Compounds,2025,936:178674.

[4] Ayed A, Bras G, Bernard H, et al. Additive Manufacturing of Ti6Al4V with Wire Laser Metal Deposition Process[J]. Materials Science Forum,2021,923:117-124.

[5] SINGH S, SHARMA S K, RATHOD D W. A Review on Process Planning Strategies and Challenges of WAAM[J]. Materials Today: Proceedings,2021,47:6564-6575.

[6] Lu, B.H. (2020). Additive Manufacturing—Current Situation and Future. China Mechanical Engineering, 31, 19-23.

[7] Ahmet Suat Yıldız,Barış Koc,Oğuzhan Yılmaz. "Thermal behavior determination for wire arc additive manufacturing process." Procedia Manufacturing (2021).

[8] Lawal S·L, Afolalu S·A. Effect of Welding Process Parameters on the Mechanical Properties of TIG and MIG Welds in HSS X65 Pipe-A Review[J]. IOP Conference Series: Earth and Environmental Science, 2024, 1234: 012001.

[9] Zhang Jintian, Wang Xinghua, Wang Tao, et al. Study on single-pass single-layer process characteristics of arc additive manufacturing[J]. Materials Review, 2020, 34 (24): 24132-24137.

[10] Wan Xiaohui, Jia Zhihong, Guo Delun. Optimization of ultra-high frequency arc additive manufacturing process based on response surface methodology[J]. Transactions of the China Welding Institution, 2020, 41 (6): 45-50.

[11] Ni Yongqian, Wang Meng, Du Xinwei, et al. Arc additive manufacturing weld bead size prediction model based on genetic algorithm optimization[J]. Mechanical Manufacturing Abstracts: Welding, 2021 (6): 12-17.

[12] Yang Zou,Shaoqi Shi,Zefeng Yang,Teng Xu,Yongqi Liang. "Multi-objective optimization of key process parameters in laser cladding Stellite12 cobalt-based alloy powder." Journal of Laser Applications (2023).

[13] Cui Lujun, Liu yaxuan, Guo Shirui, et al. Prediction of Laser Cladding Layer Cross-Sectional Morphology - Based on SSA-BP Neural Network[J]. Optik,2022,254:168624.

[14] Liang Yandong, Xu Yuan, Jia Meng, et al. Experimental study on the influence of an alternating magnetic field on the CaCO3 fouling of a heat transfer surface[J]. International Journal of Heat and Mass Transfer,2022,191:123096.

[15] Heng Xia,Jian Tang,J. Qiao. "Deep Forest Regression Based on Dynamic State Transition Optimization Algorithm." 2020 Chinese Automation Congress (CAC) (2020).

[16] Zou Yang, Shi Shaoqi, Yang Zefeng, et al. Multi-objective optimization of key process parameters in laser cladding Stellite12 cobalt-based alloy powder[J]. Journal of Laser Applications,2023,35(2):022009.

[17] Zhang Yuhang, Cheng Wangjun, Sun Yaoning, et al. Surface Quality Optimization of Laser Cladding Based on Surface Response and Genetic Neural Network Model[J]. SSRN Electronic Journal,2022(1):1-10.

[18] Liang M, Wang Chenglei, Cai M, et al. Study on optimization of laser cladding process parameters of aluminum alloys using a prediction model of the neuralgenetic algorithm[J]. Journal of Physics: Conference Series,2021,1813(1):012036.

[19] Shiwei He,Zhiqiang Zhang,Hanxi Li,Tiangang Zhang,X. Lu. "Multi-Objective Optimization for Forming Quality of Laser and CMT-P Arc Hybrid Additive Manufacturing Aluminum Alloy Using Response Surface Methodology." Actuators (2024).

[20] Van Thao Le,Quang Thanh Doan,Dinh Si Mai,Manh Cuong Bui,Hoang Son Tran. "Prediction and optimization of processing parameters in wire and arc-based additively manufacturing of 316L stainless steel." Journal of the Brazilian Society of Mechanical Sciences and Engineering 9(2022).

[21] Zhao Pengkang, Fang Kui, Tang Cheng, et al. Effect of interlayer cooling time on the temperature field of 5356-TIG wire arc additive manufacturing [J]. China Welding: English Edition, 2021, 30 (2): 114-121.

[22] Jinshun Cao,Xuan Sun,Zi-xian Lin,Quancheng Dong. "Dimensional modeling of single pass welding in wire and arc additive manufacturing." International Conference on, (2023).

[23] Liu Lixiang, Zhou Xiangman, Zhang Haiou, Bai Xingwang. "Weld bead profile model function for arc additive manufacturing multi-layer single-pass deposition." Transactions of the China Welding Society 6(2020).

[24] Zhao Jiali. Based on the single-layer contour pattern, the comparison of the zigzag parallel hatch and the contour parallel hatch[J]. Journal of Physics: Conference Series,2021,1948(1):012013.

[25] Bui M C, Le V T, Ta D X, et al. Thermal Analysis in Wire Arc Additively Manufactured SS308L Walls via Numerical Simulations[J]. Procedia Manufacturing,2021,55:143-150.

[26] Chen Shujun, Wang Xuan, Xu Min, et al. Research on the forming law of Al-Zn-Mg-Cu alloy based on TIG three-wire arc additive manufacturing[J]. Hot Working Technology, 2021, 50(1):87-91.

[27] Liu, D., Lü, Y., Yang, H., Zhou, W., & Yuan, F. (2020). Effect of Arc Additive Process Parameters on Forming Quality. Mechanical Science and Technology for Aerospace Engineering, 39(9), 1412-1418.